Abrupt shifts between wet and dry phases of the 1875 eruption of Askja Volcano: microscopic evidence for macroscopic conduit dynamics

R.J. Carey [a,*], B.F. Houghton [a], T. Thordarson [b]

a Department of Geology and Geophysics, SOEST, University of Hawai`i, Honolulu, HI 96822, USA

b School of GeoSciences, University of Edinburgh, Edinburgh EH9 3JW, United Kingdom

* Corresponding author. Tel.: +1-808-956-5960 Fax: +1-808-956-5512

e-mail address: beccarey@hawaii.edu

Abstract

The eruption of Askja in 1875 was a powerful eruption with intervals of sustained activity on time scales of hours, yet also with abrupt shifts in eruption style, e.g. from dry to wet fall, and from buoyant to collapsing column conditions, and sharp fluctuations of eruption intensity in every major eruptive phase. Deep ascent processes, including decompression, bubble nucleation and early growth of bubbles were similar for the four main phases, regardless of wet or dry, buoyant or collapsing column conditions. Uniformly high vesicle number densities amongst all analyzed clasts suggest that magma degassing throughout the eruption was a highly disequilibrium process creating very high bubble nucleation rates; power law size distributions of the subpopulations of small bubbles on cumulative number density plots suggest continuous nucleation of bubbles. Shallow magma ascent and bubble growth were at times decoupled from deep ascent processes; at the onset of each phase, the erupted magma appears to have a mature vesicle signature, suggesting portions of the magma experienced extended residence times in the shallow conduit, irrespective of decompression or magma ascent rate. In subsequent samples for each phase, the textural and vesicularity data suggest more uniform conditions of ascent and shallow degassing. The greater textural maturity in magma erupted at the start of each phase appears linked to shifts in vent position during two pauses in the eruption. We suggest that magma during this eruption was intruded in an elongated dike-like geometry and vent migrations between phases led to the eruption of magma that had slightly greater residence time and hence more mature textures at the start of each new phase. The major yet reversible shifts between 'dry' or magmatic and 'wet' or phreatomagmatic eruption styles were driven by changing external conditions-the migration of the vent into and out of water sources-rather than by changes of magma flux. The shift between buoyant phreatoplinian wet plume conditions and the production of wet density currents is thought to be a function of vent widening during the phreatoplinian phase, thereby decreasing the exit velocity of the wet mixture. In terms of the role of external water in the phreatoplinian phase, our qualitative textural observations and quantitative data suggest that the magma was a foam prior to fragmentation. However present data cannot resolve the exact role of the external water.

1. Introduction

Shifts between eruption styles, and changes of eruption intensities and degrees of interaction with external water are common features of high intensity silicic eruptions (e.g. Vesuvius 79AD, Sigurdsson et al., 1985; Hekla 1104 AD, Larsen et al., 1977; Taupo 181 AD; Houghton et al., 1995). Many eruptions exhibit a phreatomagmatic opening (e.g. Vesuvius 79AD, Sigurdsson et al., 1985; Taupo 181 AD, Houghton et al., 1995; Kaharoa 1305 AD, Nairn et al., 2003) and/or a shift from fall to flow conditions at the end of an eruption (e.g. Vesuvius 79 AD, Sigurdsson et al., 1985; Pinatubo 1991, Rosi et al., 2001; Taupo, 181 AD, Houghton et al., 1995). However, sharp fluctuations of eruption intensity and abrupt and reversible shifts between magmatic and phreatomagmatic styles, or fall and flow activity within sustained eruptions occur in far less systematic fashion and hence, are far more difficult to predict. Are such shifts driven by (i) conditions in the magma chamber, (ii) conduit dynamics, (iii) external factors, or some combination of these? Vesicularity studies of pumice have already been shown to provide a window into conduit dynamics, in particular the relative roles of nucleation, growth, coalescence and collapse of vesicles in the conduit in 'driving' explosive eruptions (e.g. Klug et al., 2002; Adams et al., 2006; Houghton et al., 2003; Sable et al., 2006). External factors such as conduit and vent geometries, inferred from field mapping and componentry, also have a strong influence on eruption dynamics (e.g. Wilson et al., 1980; Smith and Houghton, 1995; Mitchell, 2005), particularly on the mass discharge rate and eruption regime (e.g. Taupo 181 AD, Kaharoa 1305 AD, Furnas 1630, Azores; Cole et al., 1995). However the triggers for such abrupt shifts in style or intensity and the relative roles of external and internal factors remain poorly understood for many eruptions.

In this study, we examine in detail the products of four contrasting phases of different intensity and style during the sustained 1875 eruption of Askja volcano. Our study focuses on changes occurring within the conduit and vent environment both between, and within single phases.

We aim to address the following questions through studies of vesicle populations and vesicularities of representative pumice clasts: First, were abrupt shifts in eruption style caused by changing conditions of magma ascent or were external factors such as vent location and geometry important? Second, what mechanisms drove shorter-term

fluctuations of eruption intensity on scales of minutes to tens of minutes? Third, what caused pauses in the eruption sequence?

1.1 Geological setting

Askja is the central volcano of the Askja volcanic system situated in the northern Volcanic Zone (NVZ) in Iceland, which delineates the divergent plate boundary in north Iceland. The volcanic system is 10 – 15 km wide and 100 km long, and the central volcano hosts three calderas, the second oldest (Askja caldera ~ 10 ky) of which is 7 x 7 km wide and almost completely in-filled with post-glacial basaltic lavas (Fig. 1).

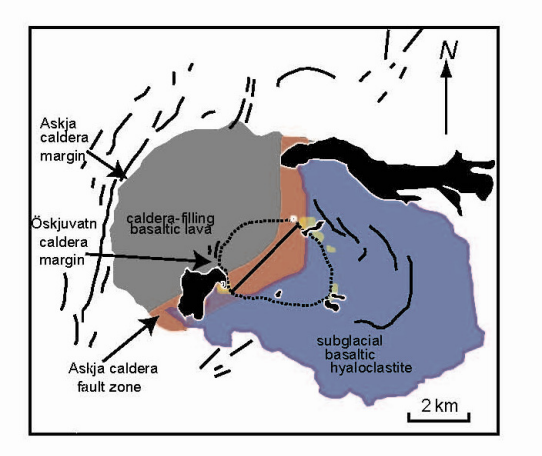

Figure 1: Map of the Askja volcano, including sites (black) of explosive and effusive basaltic volcanism post-dating the 28th – 29th March 1875 event and known vent sites of precursory activity in yellow. The volcano has two separate areas of contrasting geology; a mostly subglacial hyaloclastite formation that surrounds the Askja caldera (purple), and the Holocene basaltic lavas that partly in-fill the older Askja caldera (dark grey). The bounding fault of the older Askja caldera is shown; its position on the eastern side prior to March 1875 is highlighted by the red-shaded area. Dark lines denote lineations of the tectonic fabric of the region and ring fractures surrounding Öskjuvatn. Note that most of the pre- and post-1875 activity is focused on older Askja caldera fault margin, except for those situated on ring fractures of the younger caldera.

The youngest caldera, Öskjuvatn, is 3 x 4 km in diameter and formed after the powerful rhyolitic main phase of the eruption on 28th – 29th March, 1875. Post-glacial eruptive activity at Askja has produced extensive basaltic eruptions on ring fractures surrounding the calderas, in addition to flank eruptions (Sigvaldasson, 1979, 2002; Thordarson et al., in prep). The 1867 – 1876 volcano-tectonic event which culminated in the main phase of the eruption appears to be the result of lithospheric extension producing an en echelon array of north-northeast to south-southwest trending fissures that cut the main caldera

fault and ring fractures (Brandsdottir, 1992; Thordarson et al., in prep). All the pyroclastic vents that were active during the 28th – 29th March 1875 sequence are located within the present-day Lake Öskjuvatn (Carey et al., in review).

1.2 Eruption Summary

On March 28th 1875, the eruption of Askja began and lasted for approximately 17 hours, depositing tephra (0.33 km^3 dense rock equivalent DRE) over eastern Iceland, Scandinavia and northern Germany (Sparks et al., 1981; Carey et al., in review). This eruption also produced 0.01 km^3 (DRE) of dilute pyroclastic density current deposits which were mostly confined to within the caldera. The main eruption began at 9 pm with a subplinian phase with a duration of approximately one hour. This phase produced a reversely graded, coarse pumice fall deposit. Underlying this layer at many proximal/medial locations is a thin very fine pumiceous ash that may reflect a brief phreatomagmatic opening to the main eruption. After a pause in activity of approximately nine hours, a wet intense phreatoplinian phase began from a separate vent to the north west of the subplinian vent and lasted for approximately one hour (Thordarson et al., in prep; Carey et al., in review). This abrupt shift in style and intensity marks the first sharp change in eruption dynamics. The sustained phreatoplinian column produced fall deposits with minor intercalated dilute density current deposits confined within the caldera and attributed to slight fluctuations in eruption intensity and water-magma ratio (Carey et al., in review). After the phreatoplinian phase, farmers in eastern Iceland observed a two hour-long pause in activity between the phreatoplinian and the subsequent Plinian fall (Thordarson et al., in prep), however in the proximal environment dilute density currents were emplaced at this time. This abrupt shift from wet sustained buoyant plume conditions to a collapsing column is the second major change in eruption dynamics. The pyroclastic density currents are inferred to have originated from the phreatoplinian vent and their characteristics change with time, becoming ash-poor and well sorted, with bedforms that have increasing wavelengths and amplitudes. Strong seismicity then accompanied a second shift in vent location and the onset of the main Plinian phase characterized by a sustained high eruptive plume which lasted for approximately five to six hours (Carey et al., in review). The beginning of this final phase marks the third major shift in eruption dynamics in the main eruption.

1.3 Eruption stratigraphy

Initial studies conducted by Self and Sparks (1978), recognized that this eruption was one of few that included powerful sustained phreatomagmatic activity for which they coined the phrase 'phreatoplinian'. Self and Sparks (1978) proposed an initial stratigraphy of the products from the main, pre- and post-eruptive events based on the proximal products, dividing the entire stratigraphy into eight units. Four of these units were produced during the main eruption on March 28th – 29th 1875. Sparks et al., (1981) developed the framework for the eruption with studies of the proximal, medial and distal areas in Eastern Iceland, in addition to integrating historical records of the eruption. Further studies conducted by Carey et al., (2008a) adapted the original stratigraphic nomenclature of Sparks et al., (1981) but divided the dilute density current deposits (C2) into three main flow units and identified five sub-units within the proximal Plinian unit D (Fig. 2).

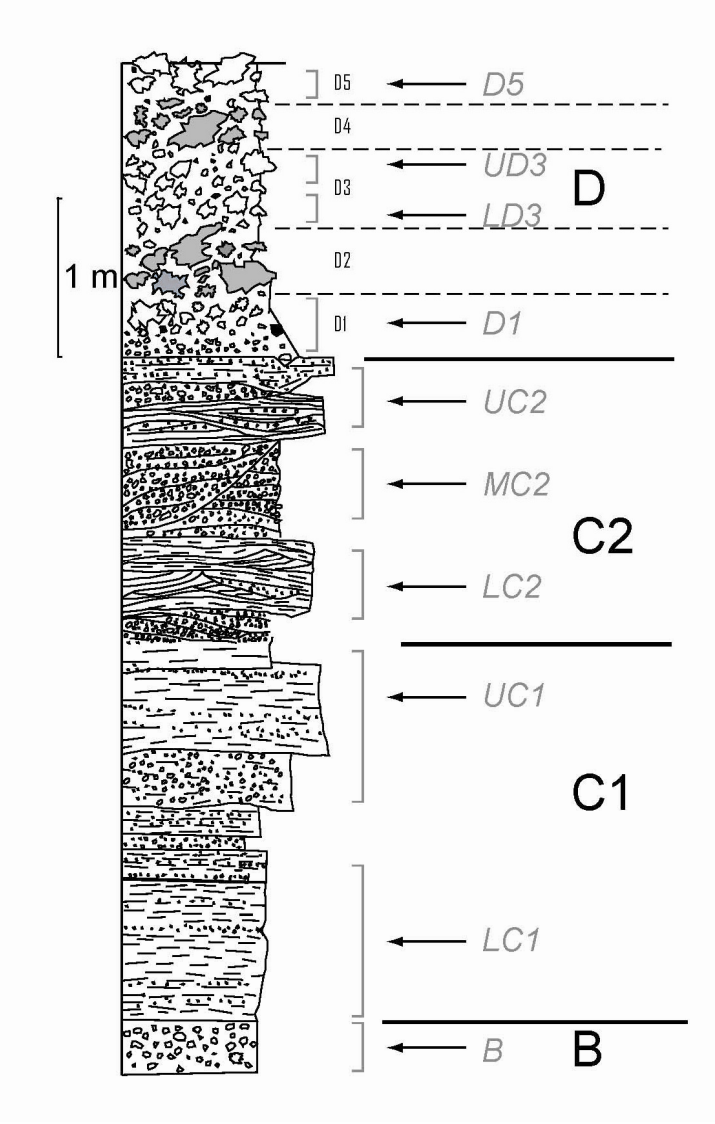

Figure 2: The stratigraphy of the deposits formed in the main eruption (28th – 29th March 1875). This stratigraphy was originally adapted from Self and Sparks (1978) and Sparks et al., (1981) with revision by Carey et al., (in review). Ten samples were taken from these four units for vesicularity studies (as shown by grey brackets).

1.4 Deposit characteristics

The March 28th – 29th 1875 deposits are well exposed along the caldera rim, and fall units are dispersed toward the east (Sparks et al., 1981; Carey et al., in review). The first unit B is a subplinian fall deposit (0.004 km^3 DRE), with a more limited dispersal than the following fall phases. This unit is a well-sorted pumice fall deposit.

The phreatoplinian fall deposit C1 directly overlies the subplinian fall deposit and is dispersed over eastern Iceland and extends to Scandinavia, where it merges within the overlying Plinian fall (e.g. Sparks et al., 1981; Carey et al., in review). Grain size analyses conducted by Sparks et al., (1981) suggest that 99 wt% of this deposit is finer than 1 mm. The dilute density current deposits of C2 were emplaced following the cessation of phreatoplinian fall and are largely confined to the caldera. Carey et al., (in review) observed three units within the C2 deposits in the proximal area based on the abundance of ash, presence of well-sorted lapilli beds, and bedform wavelength, angle and amplitude. Consequently these have been named lower (LC2), middle (MC2) and upper (UC2), adhering to the original Sparks et al., (1981) nomenclature. In the proximal region, the overlying D Plinian deposits can be divided into five separate sub-units; D1, D2, D3, D4 and D5. D1, D3 and D5 are widespread tephra falls, with thinning half-distances (B_t) of 3 – 4 km, whereas the D2 and D4 deposits have B_t values one to two orders of magnitude less (10s to 100s of meters; Carey et al., 2008a). These more locally dispersed sub-units were inferred to have been produced by separate vents further to the north that had a fountaining eruption style (northern *W* on Figure 3) (Carey et al., 2008a, b). In the medial and distal environments, D1, D3 and D5 merge into a single reversely graded fall unit (unit D). The Plinian D deposits are also dispersed over eastern Iceland and extend over to Scandinavia (Sparks et al., 1981; Carey et al., in review).

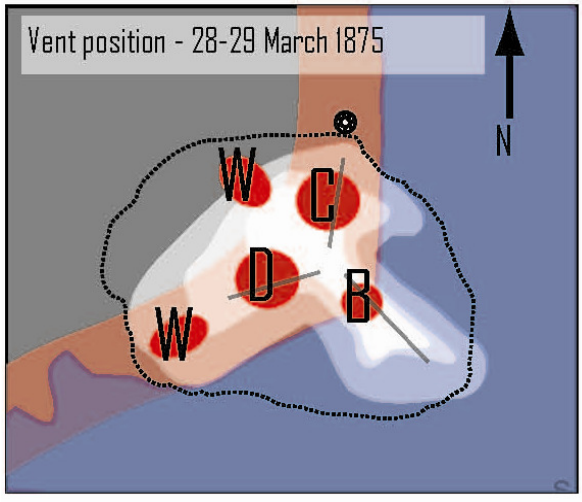

Figure 3: The present day form of Öskjuvatn caldera (dashed line). Also shown in white is the early form of the post-eruption depressions and Öskjuvatn caldera in 1876 as reconstructed by Jónsson (1942), based on descriptions made in 1876 by Johnstrup (1877). The observations document a triangular depression, with three fracture swarms: one to the southeast, one to north and one to the west-northwest (Watts, 1876; Jöhnstrup, 1877, 1876). The 'small pond' of water described in these reports was located at the junction of these two depressions. B, C and D, are our inferred vent positions: W are the locations for fountaining vents during the D phase (Carey et al., 2008a, b). The older Askja caldera marginal fault is shown in red and the areas of contrasting basement geology are as shown in Figure 1.

1.5. Summary of eruption dynamics

The wealth of historical drawings and descriptions made prior to, during and after the main eruption is an extra source of important information that is rarely available to volcanologists working on other early historical eruptions. These observations, together with modern techniques used to calculate deposit volumes, and eruption intensities etc, allowed Carey et al., (in review) to estimate durations and constrain accurately the chronology and intensities of each phase of the eruption. Here we summarize each change in eruption dynamics as detailed by Carey et al., (in review) (Table 1).

Eruptive phase	sub-unit	Duration	MDR kg s^{-1}	VDR m^3 s^{-1}	Deposit description, changes within phases
Plinian D	D5				
Plinian D	UD3	5.5 hours	2.5×10^7	6.9×10^4	Vent opening phase, sustained throughout duration
Plinian D	LD3		3.5×10^7 (peak)	9.5×10^4	reverse grading suggests increasing intensity with time
Plinian D	D1	peak 4 hours			
PDC C2	UC2				Episodic changes of mass flux, dilute density currents spread
PDC C2	MC2	2 hours	2.3×10^6	3.9×10^3	radially from a point source. Currents become dryer with time,
PDC C2	LC2				suggesting decreasing influence of water
Phreatoplinian C1	UC1	1 hour	6.8×10^7	1.2×10^5	Vent opening phase, short-lived instabilities of plume margins
Phreatoplinian C1	LC1				due to minor fluctuations of mass flux and magma-water ratio
Subplinian B	B	1 hour	2.6×10^6	3.9×10^3	Vent opening phase, sustained throughout duration
					increase in intensity with time

Table 1: Summary table of eruption characteristics taken from Carey et al., (in review) for the four phases of the main 1875 eruption.

1.6 Vent location and timing

Vents active throughout the main eruption are presently located within Lake Öskjuvatn. Observations made after the main eruption document a triangular depression with three fracture swarms extending outwards from the centre of the depression: one to the southeast, one to north and one to the west-northwest (Fig. 3; Watts, 1876; Johnstrup, 1877, 1876). Carey et al., (in review) positioned the vent locations within this depression (Fig. 3).

The B subplinian vent was located within the NW-SE trending fault swarm and is the eastern-most vent position throughout the eruption (*B* on Figure 3). The circular patterns for the proximal C1 phreatoplinian isopleths and isopachs are difficult to interpret in terms of a vent position (Carey et al., in review). However, the wet nature of the C2 density currents suggests that they were erupted from a similar position to the vent producing C1 (*C* on Figure 3), and flow directions for the density currents point to a

central north region in the present-day lake, which is within the upper portion of the old caldera fault region. Descriptions of a small pre-existing pond of surface water are also coincident with this location**.** Sharp unconformities between the pyroclastic density currents and the Plinian deposits suggest severe ground shaking in between these two phases, in accordance with a further shift in vent location at this time. Componentry and dispersal data of unit D deposits suggest a vent location in the mid to southern extent of the old caldera fault region (*D* on Figure 3) (Carey et al., in review).

1.7 Chemistry

Petrological and geochemical studies of the 1875 deposits were conducted by Sigurdsson and Sparks (1981), Sigvaldasson (1979) and Macdonald et al., (1987). The bulk of the magma erupted during the main phase varied in silica content (whole rock SiO_2: 68 – 75 % and glass SiO_2: 70 – 75 %), however no systematic patterns of changing silica content with time were observed. The phenocrysts are typically less than 1 mm in diameter, unzoned and subhedral to round, and contain common inclusions of pale brown rhyolite glass (Sigurdsson and Sparks, 1981). Geothermometry studies by Sigurdsson and Sparks (1981), suggest crystallization temperatures of 990 – 1050 °C. Phase relations indicate crystallization in water saturated conditions (P_{H_2O}) = 50-100 MPa, corresponding to saturated water content of 3 wt%. The petrological data have been interpreted to indicate pre-eruptive injection of fresh basaltic magma into a crustal reservoir beneath Askja, heating and partly mixing with an existing rhyolite body at the top of the reservoir, thereby triggering the climactic eruption on 28^{th} – 29^{th} March 1875 (Sigurdsson and Sparks, 1981).

2.0 Methods

At two proximal sections, ten samples were collected throughout the stratigraphy of the main phase, each containing at least 100 pumice clasts in the 16 to 32 mm size range. One sample was collected from unit B, two samples from upper and lower C1, three samples from C2 and four samples from D (Fig. 2). We chose not to collect samples from the D2 and D4 sub-units, due to contamination by pumices from other vents (Carey et al., 2008a, b).

Clasts in each of the samples (B, LC1, UC1 etc.) collected throughout this eruption were separated into two end-member groups; clasts that had an elongated fabric, i.e. consisting of stretched tube vesicles (tube pumices) and clasts that had no fabric, i.e. with a heterogeneous assortment of bubble sizes and equant, broadly elliptical shapes (equant pumices) (e.g. Pollacci et al., 2001, 2003).

The bulk densities of these pumices were measured using the techniques of Houghton and Wilson (1989) and converted to vesicularities using an average bulk density of 2350 kg m^{-3} based on density measurements of 1875 rhyolitic obsidian. The distribution of densities for each sample was plotted on histograms so that individual clasts could be chosen for microtextural studies. We selected 5 - 10 pumice clasts from each sample representing the mode and low/high vesicularity tails. The largest clasts were chosen from each density bin and cut to attain the maximum thin-sectional area. Care was taken not to thin section pumices with elongated (or tube-like) vesicles. The lowest magnification images (4.5x) were collected by scanning the thin sections on a Hewlett-Packard flatbed scanner at 1200 dpi resolution and used to measure the largest vesicles in the pumices. Eighteen backscatter electron images from each clast were taken on a JEOL-5900LV scanning electron microscope operating at a 20 kV accelerating voltage and 1 nA beam current. The images were then transformed into binary images in order to measure bubble diameters in two dimensions (for image magnifications of 4.5x, 25x, 100x, 250x, 500x). Two-dimensional size distributions (number per unit area, N_A) were then converted to volume distributions (number per volume, N_V) using the stereological conversion method of Sahagian and Proussevitch (1998). Vesicle number densities were recalculated with reference to the melt volume (N^m_v) to avoid underestimating bubble number densities of highly vesicular samples (after Klug et al., 2002). The Askja pumices contain < 0.5% phenocrysts and no microlites (Sigurdsson and Sparks, 1981) and thus crystal abundance and size distributions were assumed to be negligible.

3.0 Results

3.1 Clast textures

Samples generally had < 30 wt.% of tube pumices, however for the final C1 sample, two pyroclastic density current (MC2, UC2) and the final D samples (D5), percentages were between 41 and 74 wt.% (Table 2).

Eruptive Phase	sub-unit	equant no.	tube no.	equant wt%	tube wt%	mean density kgm^{-3}	3 min kgm^{-3}	3 max kgm^{-3}
Plinian D	**D5**	31	69	26	74	580	270	1130
Plinian D	**UD3**	69	31	73	27	350	210	620
Plinian D	**LD3**	70	30	72	28	330	190	600
Plinian D	**D1**	81	19	79	21	400	190	730
PDC C2	**UC2**	53	47	53	47	320	190	570
PDC C2	**MC2**	42	58	33	66	320	150	640
PDC C2	**LC2**	78	22	79	21	330	120	890
phreatoplinian C1	**UC1**	68	32	58	41	310	180	680
phreatoplinian C1	**LC1**	73	27	73	27	380	220	740
subplinian B	**B**	79	21	81	19	340	170	590

Table 2: Textural and density data for each sample taken from the 1875 eruption deposits. The number and wt% of tube vs. equant pumices in each sample are listed, in addition to the mean, average of the three minimum and average of the three maximum clasts. The grey shaded samples are observed to have higher abundances of tube pumices than samples at the onset of a phase.

3.2 Clast density and vesicularity

All the samples are all extremely unimodal in comparison to other Plinian eruptions, typically with very narrow ranges of clast density (total range 200 – 1200 kg m^{-3}; 41-92 % vesicularity) and low density modal peaks (300 – 600 kg m^{-3}; 75-87 %) (Fig. 4a; Table 2).

The unit B sample is unimodal with a mean density of 340 kg m^{-3} (85 %) and a very narrow range of density values (160 – 610 kg m^{-3}; 74-93 %). The transition between subplinian and phreatoplinian phases (after a ~9 hour-long pause) is marked by a widening of the range of density values (220 – 850 kg m^{-3}; 63-91 %; Fig. 4b) and a slight increase in the mean density (380 kg m^{-3}; 84 %) but a similar modal density (Fig. 4a; Table 2). In upper C1, the mean density decreases to 310 kg m^{-3} (87 %) and the range of density values decreases dramatically, with the narrowest distribution of density of the entire eruption (160 - 440 kg m^{-3}; 81-93 %; Fig. 4b) .

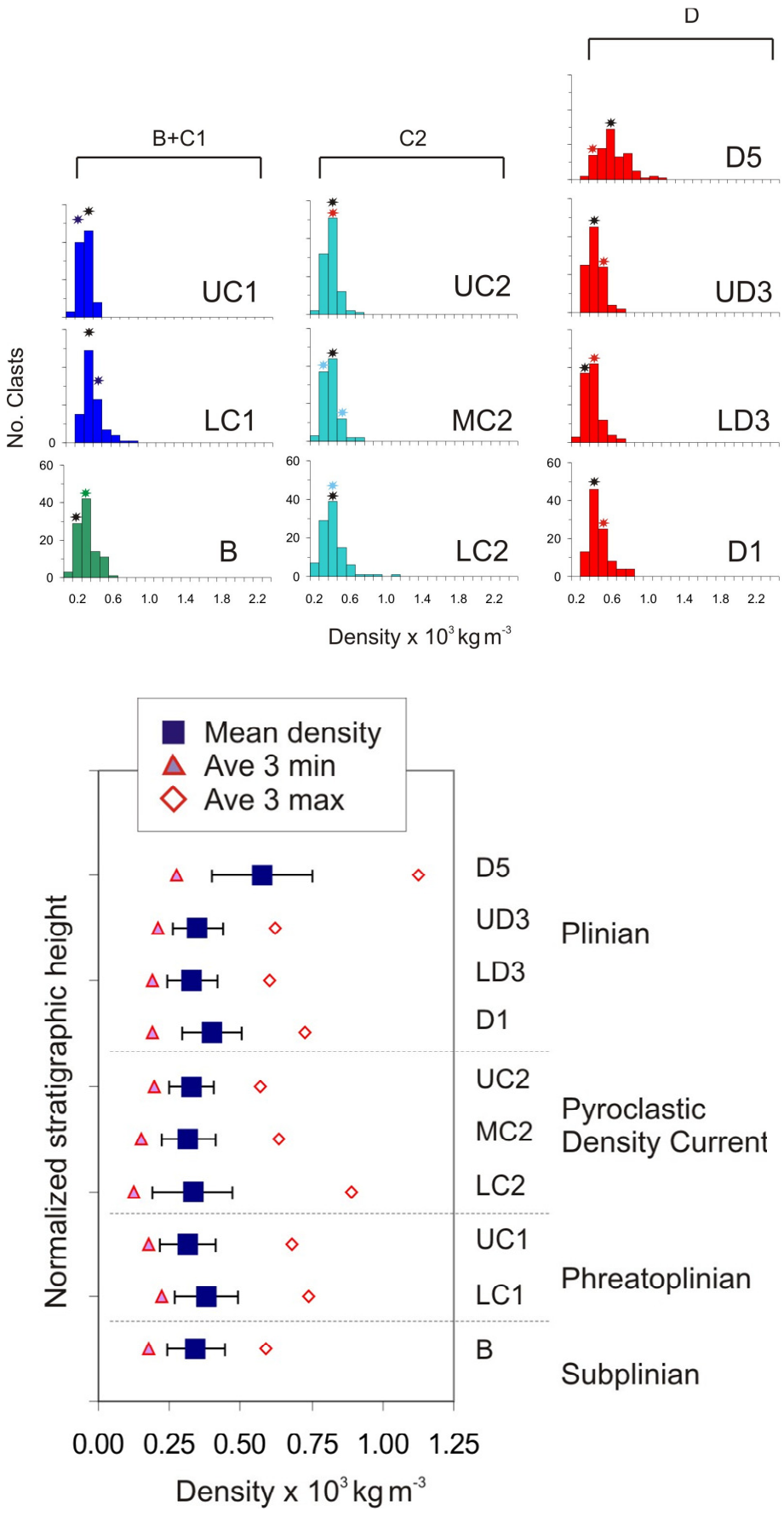

Figure 4: a) Clast density histograms from each of the 10 samples identified in Figure 2. The stars show where representative clasts were taken from for qualitative textural analyses. The black star is the location of the pumice clast used in the quantitative analyses for each sample. The selected clast is representative of the bulk of the magma erupted at that time, due to its location for most clasts on the modal peak, in addition to the narrow unimodality of most clast histograms. Note the similarity of clast histograms from the wet phreatoplinian and dry Plinian samples. **b)** Sample density distribution vs. normalized stratigraphic height for ten samples collected throughout the density clasts have been plotted for each sample, in addition to one standard deviation of the mean density. Note at the onset of a phase, a greater mean and range of clast densities skewed to higher values are apparent, as well as a reduction in the range of clast densities as a phase progresses. The final Plinian sample, which represents the end of the eruption also shows an extended density range and the highest mean density of any of the samples.

The first pdc sample has the widest range of density seen in the first half of the eruption (180 - 1100 kg m^{-3}; 53-92 %), but similar mean density values (330 kg m^{-3}; 86 %). From LC2 through MC2 to UC2, the range of density values decreases, skewed to lower density clasts (180 – 620 kg m^{-3}; 74-92 %; Fig. 4b), the mean density decreases slightly (320 kg m^{-3}; 86 %), however the modal density remains similar (Fig. 4a; Table 2). The switch to Plinian activity is marked in the clast density data by an increase in the range of clast density, skewed to higher density clasts (250 - 740 kg m^{-3} 69-89 %), coupled with an increase in mean clast density (400 kg m^{-3}; 83 %) . The D3 samples of the Plinian phase have lower mean densities (330 and 350 kg m^{-3}; 85-86 %) . The most striking shift is seen in D5 which contains the most dense clasts seen in the 1985 samples with a marked shift in both the mean and density minima to higher values (Fig. 4b; Table 2).

Interpretation

The ten density samples collected have very similar narrow unimodal peaks at relatively low densities (Fig. 4a). On a global scale, the narrow unimodality of these samples is unique (e.g. CITE OTHER REFS), suggesting that the magma ejected in each phase of the 1875 eruption was exceptionally uniform, and that within and between phases, conduit processes of ascent and vesiculation were broadly similar. The most important exception is the sample from the closing phase of the eruption, D5. Other exceptions are the histograms representing each onset of a new phase, which have broader distributions than those following within the same phase (Fig. 4a). In all four examples (D5, C1, LC2 and D1) the distributions broaden due to an influx of higher density clasts (Figs. 4a, 4b). These contrasts suggest that the magma erupted at the onset of every phase had a slightly different history. Within phases, the range of clast densities and unimodality of the density distributions both narrow with time. This trend suggests increasingly uniform conditions of vesiculation (Figs. 4a, 4b). The exception provided by the final Plinian sample (Fig. 4a) is even more important. It shows the broadest span of density data with the mode displaced significantly (Figs. 4a, 4b). This has important implications, which we explore later, for increasing heterogeneity and maturity of the magma in the closing stages of the eruption.

3.3 Vesicle data

3.3.1 Qualitative observations

Observations of vesicle textures are key to understanding roles of the vesiculation process and relative timescales of ascent and degassing (e.g. Cashman and Mangan, 1994; Mangan and Cashman, 1996). Here we describe key features of selected pumice clasts in every unit, including vesicle size, shape and habit for every unit of this eruption. Clasts were chosen to represent the bulk of the magma erupted and selected from the bins that represent the modal density range.

Subplinian unit B

Pumice textures from the subplinian phase are relatively uniform and are characterized by zones of highly coalesced, intermediate sized bubbles (75 – 175 μm) with round or concave walls and larger (> 175 μm) bubbles that have polylobate and convoluted shapes reflecting coalescence (see 100x unit B image in Fig. 5). This population of coalesced bubbles is often clustered into domains separated from one another by zones characterized by smaller (5 – 25 μm) round bubbles. Bubble walls range between 1 and 13 μm thick (predominantly 6 - 13 μm).

Phreatoplinian unit C1

There are significant contrasts in pumice textures between the previous unit B subplinian pumice and the early phreatoplinian clast (LC1) erupted approximately nine hours later. The LC1 sample has a population of much more numerous, small round 5 – 25 μm bubbles, often clustered around isolated, large coalesced polylobate bubbles, and similar abundances of intermediate-sized coalesced bubbles which show either round or complex shapes (Fig. 5). Bubble wall thicknesses range from 1 to 13 μm, but are predominantly 8 -13 μm thick. The UC1 sample has a higher abundance of 5 – 25 μm bubbles, which are round and distributed evenly around larger bubbles (75 – 250 μm) (Fig. 5). Larger bubbles commonly have irregular sharply concave shapes and broken, retracted bubble walls. Regardless of bubble size and abundance, bubble walls are thicker with respect to previous clasts ranging between 3 and 18 μm, but predominantly 8 - 14 μm (see 500x UC1 image in Fig. 5).

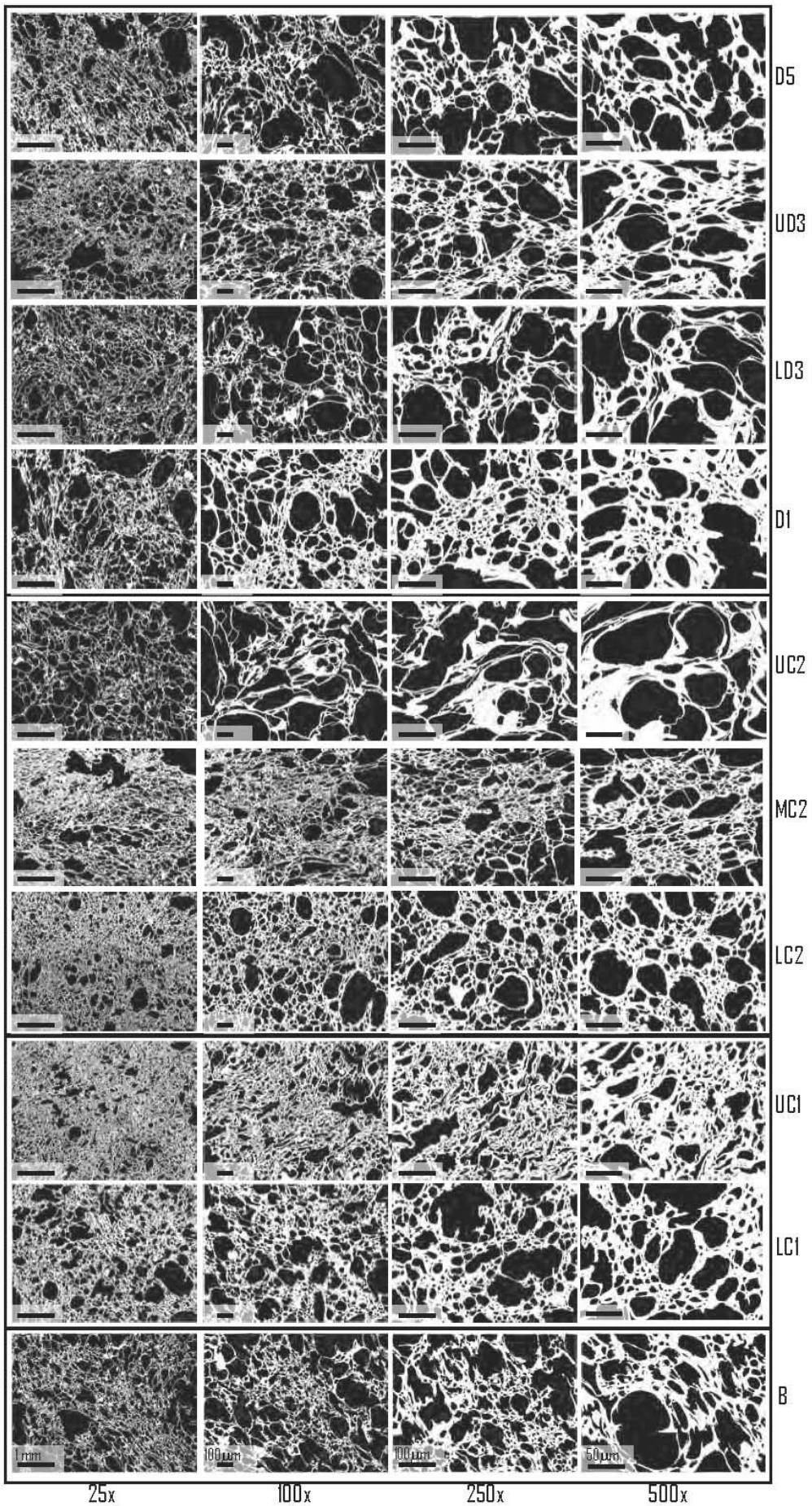

Figure 5: Scanning electron microscope images of representative pumices of the ten samples collected throughout the deposits of this eruption. The magnifications of each image are shown at the bottom of the figure. The glass is white, and the bubbles are black in each image.

Pyroclastic density current phase C2

The transition between phreatoplinian fall and LC2 density current deposits is recorded in pumice textures by a decrease in the complexity of bubble shape, a decrease in the abundance of small bubbles, and an increase in the number of intermediate-sized bubbles. Bubble wall are slightly thinner than those of UC1, ranging from 2 to 10 μm (Fig. 5). Textures in the MC2 clast are very different from the LC2 sample. Two distinct textures are observed in images: a texture characterized by intermediate to coarse bubbles that are polylobate or have complex concave walls, with very few small bubbles and relatively thin walls (2 – 8 μm); and a texture dominated by small round bubbles with thicker bubble walls (5 – 10 μm) (see 250x image in MC2; Fig.5). The textures of the UC2 clast is distinct from all earlier pumices, dominated by homogeneously distributed intermediate to large bubbles that are predominantly round to sub-round, and bubble walls that have extremely variable thicknesses. Coalescence textures, such as very thin convoluted walls, are common, in addition to smaller elongated bubbles aligned along the edges of much larger coalesced bubbles.

Plinian phase D

The transition to the Plinian phase is extreme as seen in pumice textures. The major differences between UC2 and D1 pumice textures include: an increase in abundance of both small round bubbles and larger coalesced bubbles with concave walls or polylobate shapes; development of coalescing bubble trains at the expense of the round intermediate-sized bubbles; a generally increased thickness of bubble walls (8 – 15 μm); and the separation of smaller and larger bubbles into distinct domains observed at all magnifications (Fig. 5). The LD3 and UD3 pumice textures have an increased abundance of small- to intermediate-sized bubbles, which are round to sub-angular, and minor large bubbles with irregular shapes. Bubble walls are thinner than those of the earlier pumices, but are variable, ranging from 2 to 15 μm thick (Fig. 5). The D5 clast has similar textures to those of the LD3 and UD3 pumices described above. However, the zones of intermediate to coarse bubbles dominate, the coarse bubbles are larger and extend to very coarse bubbles (> 2 mm), and the abundance of small bubbles has decreased significantly (Fig. 5). Bubble trains are common and there is a slight elongate fabric to the pumice textures.

Interpretation

Pumices from Unit B show moderate to high degrees of coalescence, and the lack of small bubbles is suggestive of a relatively mature bubble population, i.e. one reflecting extended time for bubble growth after nucleation. Textures of LC1 pumice clasts ~~,~~ suggest less time for vesiculation and a shorter residence time in the conduit than the subplinian magma (Table 3). Pumice textures change significantly within the phreatoplinian phase suggesting a complex ascent history for the late-stage phreatoplinian magma.

Eruptive phase	sub-unit	Density kgm^{-3}	Vesicularity %	N_A total cm^{-2}	N_V total cm^{-3}	N^m_V total cm^{-3}	*n* (no/cm^3/cm)	size range (microns)	Median (microns)	No. included
Plinian D	D5	580	77.6	1286	1.6E+08	7.1E+08	3.5 E+7	4 - 4883	316	1233
Plinian D	UD3	350	85.2	1549	2.0E+08	1.4E+09	3.7 E+7	4 - 3665	180	1547
Plinian D	LD3	330	88.1	901	1.2E+08	1.0E+09	1.8 E+7	4 - 3833	200	943
Plinian D	D1	400	86.2	1121	2.0E+08	1.3E+09	4 E+7	4 - 2766	350	1471
PDC C2	UC2	320	88.5	853	1.3E+08	1.1E+09	2.6 E+7	4 - 2897	350	928
PDC C2	MC2	320	86.2	2398	2.8E+08	2.0E+09	1.2E+08	4 - 4334	112	2036
PDC C2	LC2	310	86.6	1793	3.2E+08	2.4E+09	5.6E+07	4 - 4336	180	1790
Phreatoplinian C1	UC1	310	83.4	2272	3.4E+08	2.0E+09	7.1 E+7	4 - 2488	158	1764
Phreatoplinian C1	LC1	380	83.6	1682	2.4E+08	1.5E+09	6.1 E+7	4 - 3595	225	1793
subplinian B	B	290	87.8	843	1.1E+08	9.0E+08	5.5E+07	4 - 2755	360	1882

Table 3: Table of quantitative vesicle parameters for the 1875 deposits.

UC2 textures are dominated by intermediate to large coalesced bubbles and thick bubble walls. The LC2 and MC2 textures are much more heterogeneous than those of UC2, suggesting that the UC2 magma had a relatively simple and perhaps slower ascent history leading to greater residence time available for coalescence and some bubble collapse. The bimodal bubble size distribution in D1 implies a complex history of magma ascent. The textures observed in the two middle Plinian clasts (LD3 and UD3) suggest fairly uniform conditions of fast magma ascent, and relatively little time in the shallow conduit for large-scale bubble coalescence. The textures in the final Plinian clast (D5) suggest that there was time available for advanced coalescence in the shallow conduit.

3.3.2 Quantitative vesicle data

We have obtained quantitative vesicularity data from 21 clasts, each of which was taken from the unimodal density peaks identified in Figure 4a.

Vesicle number densities

Number densities for the Askja pumices are very uniform regardless of eruption style or intensity and despite the diversity of vesicle textures described in section 3.3.1 (Table 3). The pumices from the initial and final samples (subplinian B and Plinian D5) have number densities that are slightly lower than those of the remaining eight samples of the main phase. Within the remaining samples, number densities range from only 1.0 to 2.1 x 10^9 cm^{-3} compared to, for example, 1.4 x 10^8 to 3.9 x 10^9 cm^{-3} for the 79 AD Vesuvius eruption (Gurioli et al., 2005), or 3.7x 10^8 to 3.5 x 10^{10} cm^{-3} for the 6900 BP Mt Mazama eruption (Klug et al., 2002). The C1 pumices have number densities of 1.5 and 2.1 x 10^9 cm^{-3}; pyroclastic density current clastss (C2) show a progressive decrease in number densities from 2.4 – 2.0 – 1.1 x 10^9 cm^{-3}; D Plinian clasts (with the exception of the final sample D5) are very uniform, with numbers between 1.0 and 1.4 x 10^9 cm^{-3}.

Vesicle size distributions

Vesicle size distributions (VSD's) can be used to assess the changes in rates of nucleation, growth and coalescence, throughout an eruptive sequence. The vesicle size distributions are shown for all representative clasts, grouped by phase (Fig. 6). These graphs are natural log plots (ln) of population density (no. vesicles/mm^3/mm) versus equivalent vesicle diameter. With conditions of steady-state nucleation and growth, growth rate is independent of vesicle size and results in exponential size distributions, which would plot as single straight line segments on this graph (Mangan and Cashman, 1996).

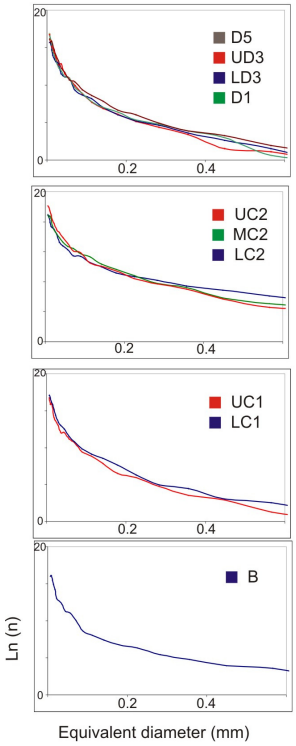

Figure 6: Vesicle size distributions (ln(n) vs. L) for all representative pumices, which have been grouped into phases. All of these clasts show one curved segment suggesting non-steady state conditions of nucleation and growth, which is similar to that observed for other silicic powerful eruptions (e.g. 6900 BP Mt Mazama, Klug et al., 2002; Vesuvius 79 AD, Gurioli et al., 2005)

Size data for each of the measured clasts of this eruption are remarkably non-linear and decline as one curved segment, similar for example, to those observed for the phreatoplinian clasts of the 181 AD Taupo eruption (Houghton et al., 2003), and the Mount Mazama pumices (Klug et al., 2002).

The size distribution of vesicles is also examined further on log plots of N^m_v (>L) versus L, where N^m_v (>L) is the melt-corrected number density (No./cm^3) of vesicles greater than diameter L. Linear trends on these graphs indicate power-law relationships between these two parameters, which is always observed for powerful silicic eruptions (i.e. Cashman and Klug, 1995; Klug et al., 2002; Adams et al., 2006) and in eruptions of basaltic composition (e.g. Gaonac'h et al., 1996; Sable et al., 2006). Each of the Askja clasts plot as two (or, in one case, three) separate line segments that each define power-law relationships (Fig. 7). For all phases, the first segment representing the smaller bubble population defines a best-fit line with slopes (i.e. exponents) between 1.6 and 2.1 (R^2 values > 0.99) (Fig. 7; Table 4). All clasts have at least one additional linear segment, with best-fit lines having exponents of 2.3 to 5.1 (Table 4). The final pyroclastic density current sample (UC2) has an extra segment, representing coarse bubbles, with an exponent of 4.4, and the transition between the two occurs at 500 μm (Table 4). The power-law distributions with 2 - 3 discrete segments suggests multiple bubble populations governed by contrasting growth laws.

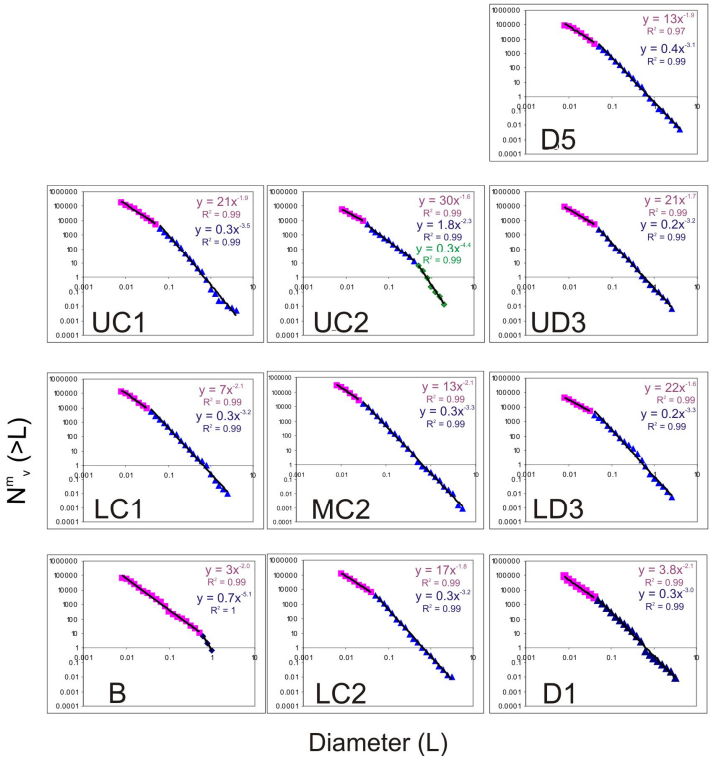

Figure 7: Log plots of N^m_v (>L) vs. L (the melt corrected number density (No./cm^3) of vesicles greater than diameter L) from all representative clstss. The first segment for all samples is shown in pink, and the power law exponent also in pink; The second segment and power law exponent is shown in blue; the third segment (UC2 only) and power law exponent is shown in green. R^2 values for each of these fits is > 0.99.

Vesicle volume distributions

Vesicle volume distributions (VVD's) also support the suggestion that all clasts have two or more bubble populations. The advantage of VVD's (where volume fraction is plotted against vesicle equivalent diameter) is that the relative contribution of each bubble size fraction to the total population can be clearly identified. This is particularly useful for identifying polymodal samples, as well as for assessing relative contributions of nucleation, growth, and coalescence processes, and for comparison with other samples. The subplinian (B) pumice has a weakly polymodal VVD, with a dominant mode at 720 μm, while weak subordinate peaks exist at 15 and 80 μm (Fig. 8). This pumice has a predominance of bubbles in the very narrow 250 μm to 1.25 mm size range, and unlike all other samples taken from this eruption, no tail of coarse bubbles greater than ~ 1.25 mm.

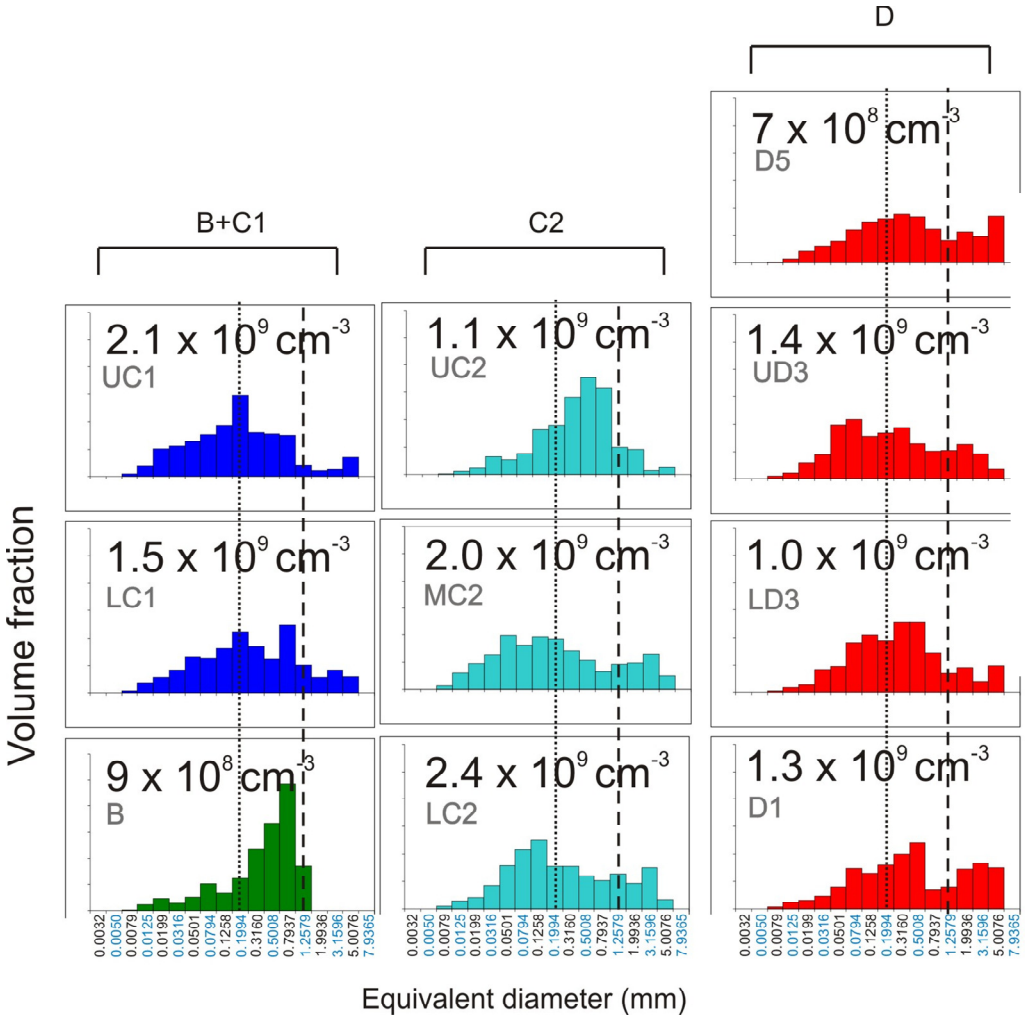

Figure 8: Vesicle volume distributions (volume fraction vs. vesicle equivalent diameter) for all representative pumices of this eruption. Vesicle number densities (in cm^{-3}) calculated for each sample are also shown top left of each graph, and two vertical lines are shown for comparative purposes between samples. Note at the onset of a new phase, a distinct population of large bubbles > 1.25 mm.

The transition between the subplinian (B) and phreatoplinian phases (LC1) is marked in the VVD's by a similar modal peak at 720 μm, but with a significant secondary peak at vesicle diameters of 200 μm, and a tail of large bubbles between 2 and 5 mm (Fig. 8). There is a much broader total range of bubble sizes, with a greater population of smaller bubbles < 125 μm. The UC1 clast also has similar populations of small and coarse bubbles. However, the higher bubble number density reflects a much larger population of bubbles < 50 μm (Fig. 8). This pumice has a unimodal peak in the main bubble population at 200 μm, no peak at 720 μm and a reduced abundance of very large vesicles extending to 5 mm.

The transition between the phreatoplinian and pyroclastic density current phases (LC2) is characterized by similar broad ranges of bubble size. However, there is a shift in the main bubble population to slightly coarser sizes and an increase in bubbles > 1.25 mm (Fig. 8). This is reminiscent of the earlier transition between the subplinian and phreatoplinian phases. The MC2 pumice has a much broader mode at smaller bubble diameters and a more sharply defined coarse mode of bubbles over 1.25 mm. The UC2 pumice has a very different vesicle volume distribution in comparison to all other pumices except for B. It is highly unimodal with a much coarser mode at ~ 400 μm and a lack of large bubbles > 1.25 mm (Fig. 8). The transition to the Plinian phase (D1) is the best-expressed example of a phase transition, with a shift from a narrow, relatively unimodal VVD dominated by intermediate sized bubbles (UC2) to a broader bi- or tri-modal VVD in D1 (Fig. 8). The D1 clast has a coarse bubble subpopulation that is more pronounced than observed in any other example, with the exception of the final Plinian sample (D5). Clasts in the Plinian phase (with the exception of D5) have broad ranges of bubble sizes, however, with time smaller bubbles become more significant especially with regard to the coarse tail (Fig. 8). The VVD of the final Plinian pumice (D5) is similar to the D1 pumice and shows bimodality, with a coarse modal peak (~5 mm), a principal broad mode at 250 μm, and a marked decrease in the relative abundance of small bubbles (Fig. 8).

The bimodal to trimodal shapes of the VVD's result in changes in slope on cumulative volume percent plots (Fig. 9). The slope of the curve reflects the narrowness of the bubble size distribution; steep slopes indicate narrow size distributions and its position

reflects the median bubble size. Sub-populations of bubbles that reflect different process (of nucleation and growth) have different slopes on these plots (Fig. 9a, b, c, d).

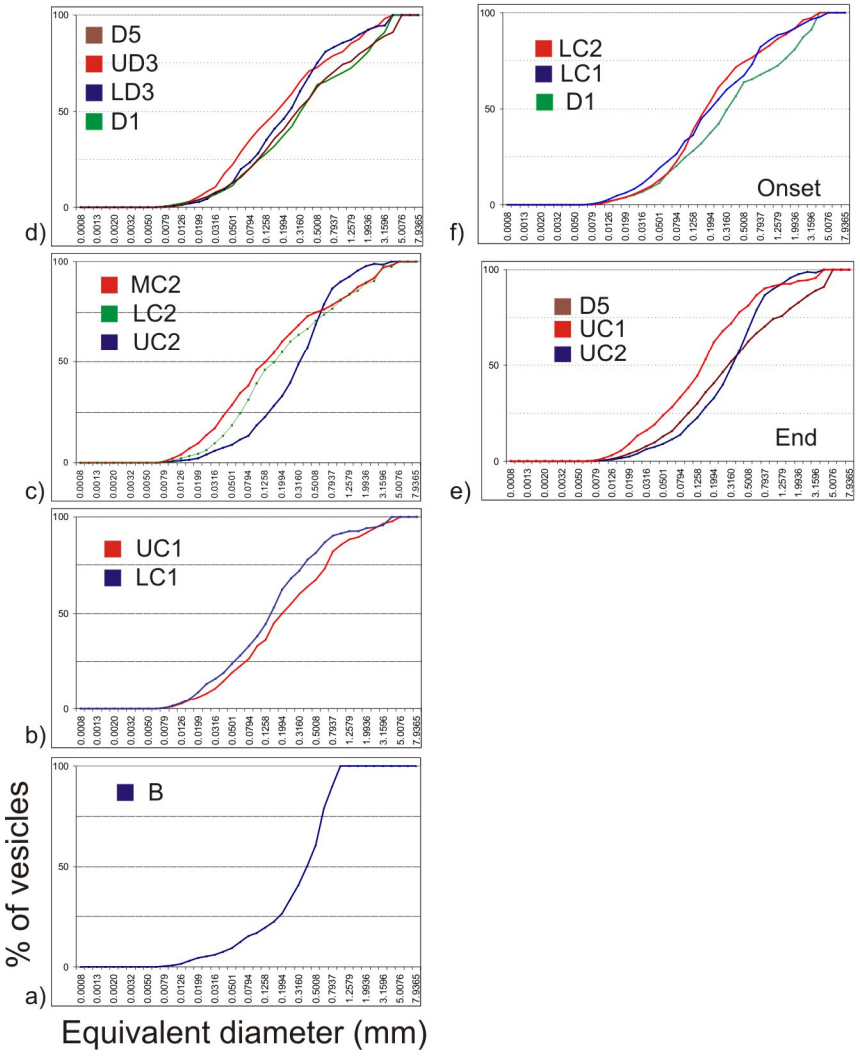

Figure 9: a, b, c, d) Cumulative volume percent plots for the modal density clasts, which have been grouped here into phases. Median diameters for each pumice have been calculated from these graphs and are listed in Table 3. **e) and f)** Samples from the onset and end of phases have also been grouped and shown here. Note the diversity of vesicle size distributions for samples reflecting the end versus onset of a phase.

Eruptive phase	Cumulative number densities - log plots of N^m_v (>L) versus L					
	point between linear segments			*power law exponent*		
	subunit	1 - 2 (μm)	2 - 3 (μm)	1	2	3
Plinian D	D5	50		1.9	3.1	
Plinian D	UD3	50		1.7	3.2	
Plinian D	LD3	39		1.6	3.3	
Plinian D	D1	50		2.1	3	
PDC C2	UC2	30	500	1.6	2.3	4.4
PDC C2	MC2	30		2.1	3.3	
PDC C2	LC2	45		1.8	3.2	
Phreatoplinian C1	UC1	63		1.9	3.5	
Phreatoplinian C1	LC1	39		2.1	3.2	
Subplinian B	B	500		2	5.1	

Table 4: **Power law exponents of individual segments as shown on plots of Nmv (>L) vs. L for each pumice clast. The bubble diameter at which the two populations (i.e. two power-law segments) join (i.e. 1 – 2) is listed.**

The subplinian sample (B) has a smooth curve with a gentle slope and no breaks in slope, indicating a single broad population of bubbles (Fig. 9a). The upper phreatoplinian sample (UC1) is steeper than that of the lower phreatoplinian sample (LC1), but has a lower median bubble size of 158 μm, in comparison to 225 μm (Fig. 9b; Table 3). The three pyroclastic density current samples (C2) show the greatest range of median vesicle sizes of the entire eruption; the two later samples (MC2, LC2) have steeper slopes, i.e., narrower size distributions, than that of the sample representing the onset of that phase (LC2) (Fig. 9c). Median vesicle sizes are much lower for the first two clasts with values of 180 (LC2), 112 (MC2) and 350 μm (UC2) respectively (Table 3). The Plinian clasts are, perhaps predictably, more uniform yet show greater complexity, as all samples show sharp breaks in slope at vesicle diameters greater than ~450 μm (Fig. 9d). LD3 and UD3 samples have smaller median diameters, reflecting more bubbles <125 μm than the early and late Plinian samples (D1 and D5) (Table 3).

From a different perspective we have plotted samples representing the onset and end of phases on the cumulative volume graphs in Figure 9e and 9f. Interestingly, the samples representing the onset of each phase are less diverse and have a greater volume% of large coarse bubbles (>630 μm) (Fig. 9e), with the exception of the sample representing the end of the Plinian phase (D5) (Fig. 9f). In addition, there is more variation in median

vesicle sizes and curve shapes at the end of a phase, reflecting the variable state of vesiculation in the final stages of each phase.

4.0 Interpretations:

4.1 Conduit processes throughout the eruption

Here we consider conduit processes over two depth ranges, arbitrarily defining deep as where processes of bubble nucleation and free growth of bubbles, by predominantly diffusion, are dominant, and shallow as the depth interval where decompressive growth and coalescence of bubbles becomes significant.

4.1.1 Implications for deep ascent processes

The narrow unimodality of density/vesicularity and vesicle number density amongst the 1875 pumices suggests that the magma ejected in each phase of the eruption was exceptionally uniform, and that within and among phases, processes and rates of early ascent, nucleation and free growth of bubbles were similar. The samples from the beginning and end of the eruption (B and D5 respectively) have the lowest number densities, which we attribute below to a greater influence of shallow processes, namely bubble coalescence.

High vesicle number densities in the 1875 pumices are strongly suggestive that the magma underwent homogeneous bubble nucleation at relatively high degrees of volatile supersaturation in a manner analogous to the eruptions of Mount Mazama 6900 BP (Klug et al., 2002), Mount St. Helens 1980 (Klug et al., 1996), and Novarupta 1912 (Adams et al., 2006) (Fig. 9). Experimental results for silicic melts show that only homogeneous nucleation at high values of supersaturation ($\Delta P > 120$ MPa) results in number densities of 10^7 to 10^9 cm^{-3} (Mourtada-Bonnefoi and Laporte, 1999; Mangan and Sisson, 2000; Mangan et al., 2004). This degree of supersaturation equates to decompression rates of 0.25 – 1.0 MPa s^{-1} (Gardner et al., 1999) and the required volatile concentrations of these silicic melts in the absence of nucleation sites were > 5 wt% H_2O and >600 ppm CO_2 (Mourtada-Bonnefoi and Laporte, 1999; Mangan and Sisson, 2000). Lower number densities of 10^6 to 10^8 cm^{-3} are more common for heterogeneous nucleation (Hurwitz and Navon, 1994; Gardner et al., 1999). The lack of efficient nucleation sites, low H_2O content and probable low CO_2 content suggests that

homogeneous nucleation was the dominant mechanism at Askja, and degassing was at a high degree of disequilibrium.

The wide range of bubble sizes in the Askja pumices, down to 5 μm, strongly suggests that bubble nucleation was an extended process continuing even after bubble-bubble interaction and coalescence affecting larger bubbles. There is some evidence supporting this from the bubble size distributions: Power-law exponents for vesicle populations reflect the processes contributing to bubble growth (Gaonac'h et al., 1996; Blower et al., 2001, 2002). The 1875 samples have multiple segments on log plots of $N^m_v(>L)$ vs. L (Fig. 9), suggesting that different processes influenced different subpopulations among the bubbles. The initial line segments characterizing the smallest bubbles have exponents between 1.6 and 2.2, (Fig. 7; Table 4). Blower et al., (2001, 2002) showed numerically that exponents ~<2 reflect continued nucleation and free growth of bubbles.

4.1.2 Implications for shallow ascent processes

We suggest, for the majority of the 1875 melt, that mid- and late-stage coalescence became a dominant process affecting the Askja magma. This process was superimposed on continued bubble nucleation and can account for the multiple linear segments identified on log plots of $N^m_v(>L)$ vs. L (Fig. 7), the broad peaks obvious on the VVD's (Fig. 8), and a coarse tail of bubbles also observed on the VVD's. The breaks between power-law segments at 30 – 50 μm on log plots of $N^m_v(>L)$ vs. L suggests that coalescence probably influenced vesicle growth for all bubbles > 30 μm and became a primary growth process from that point on. This is also observed in the sample images, where, at these typical sizes, individual bubbles begin to interact and often form bubble trains and larger irregular-shaped bubbles (Fig. 10).

The second segments on the Askja cumulative number density plots have exponents >2 suggesting the overprint of coalescence on continued nucleation (Gaonac'h et al., 1996). In particular the subplinian (B), final phreatoplinian (UC1), middle pyroclastic density current sample (MC2) and Plinian LD3 sample have the highest exponents for this second segment (5.1, 3.5, 3.3 and 3.3 respectively). Furthermore images of these samples show high degrees of coalescence with highly irregular and amoeboid-shaped vesicles that often preserve the dimensions of the smaller original constituent bubbles (Figs. 5, 11).

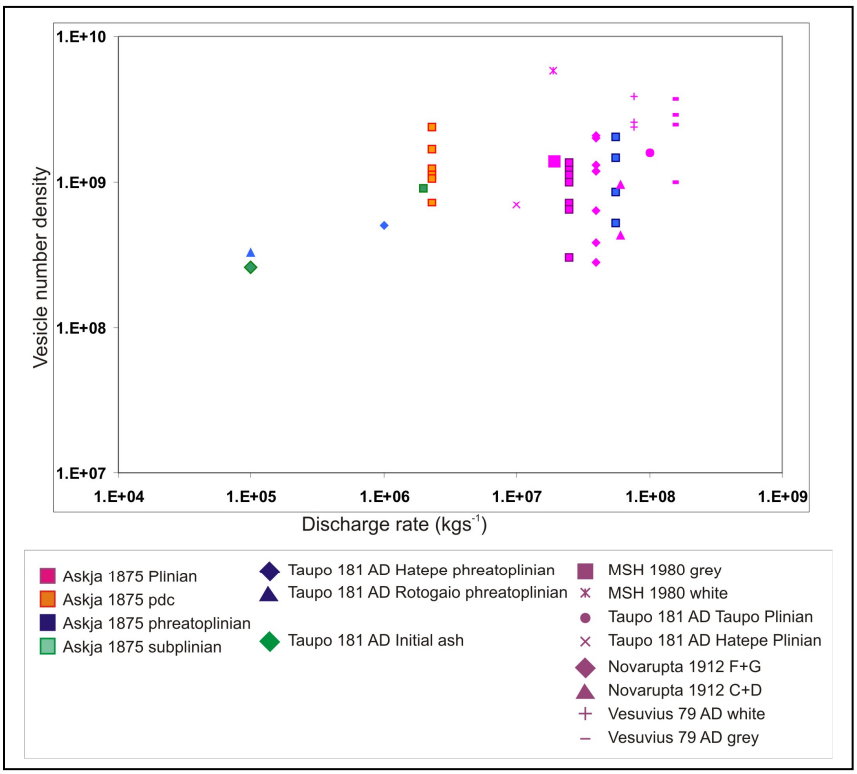

Figure 10: Vesicle number density vs. eruption intensity (discharge rate) for all Askja 1875 samples together with those calculated for other eruptions including Mt Mazama 6900 yr BP (Klug et al., 2002); Vesuvius 79AD (Gurioli et al., 2005); Novarupta 1912 (Adams et al., 2006); Taupo 181 AD, (Houghton et al., 2003); Mt St Helens (Klug and Cashman, 1994). Vesicle number densities for the Askja Plinian samples are nested within the field of other powerful large silicic eruptions, similarly to the Askja phreatoplinian samples. The Taupo phreatoplinian examples have a lower vesicle number density and lower discharge rate than those of the Askja phreatoplinian pumices.

The final pyroclastic density current sample (UC2) shows very advanced coalescence, very thin deformed bubble walls and wide bubble-poor domains (Fig. 5). This sample has a third linear segment with a power-law exponent of 4.4, also suggesting late stage growth dominated by run-away coalescence (Fig. 7; Table 4). The most distinctive clasts in this respect occur at the start and end of the main eruption (B and D5 respectively). The narrow unimodality and low modal densities of the initial subplinian phase data suggest very uniform ascent conditions throughout this phase (Fig. 4a; Table 2). The coarse median bubble size (360 μm) together with the polymodal VVD with a dominant modal peak at 720 μm suggests that coalescence was a dominant process, skewing the modal and median bubble size towards coarser values (Fig. 5, Table 3). Slower rates of magma ascent during this phase appear to have increased the relative role of coalescence and driven bubble number densities down.

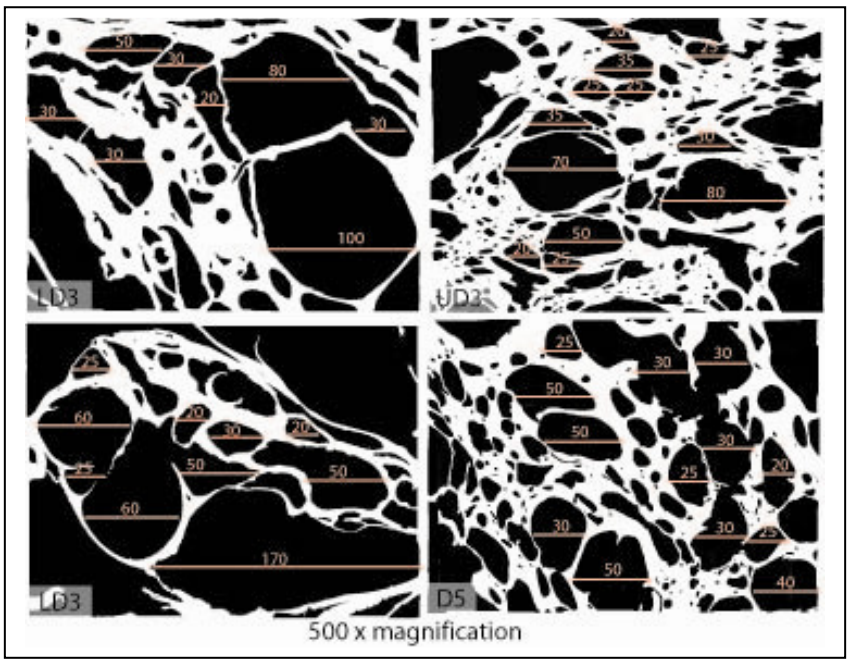

Figure 11: Four images from representative clasts taken on the scanning electron microscope at 500x magnification. The glass is white and the vesicles are black. The measurements shown are in μm. Bubble diameters are typically between 30 and 50 μm prior to high degrees of bubble coalescence between intermediate-sized bubbles. These interactions usually form large to very large bubble trains and polylobate bubbles, changing the form of the VVD and forming breaks in slope on cumulative number density plots (see Figure 7).

The final sample of the Plinian phase (D5) is unlike most other samples of this eruption. It has the lowest bubble number density, high median bubble size (316 μm), large coalesced bubble trains and high mean clast densities (580 kg m^{-3}; Table 2). These data suggest that nucleation, decompression and ascent rates declined in the final stage of this eruption, which facilitated greater residence times in the shallow conduit and hence high degrees of coalescence and partial outgassing.

4.1.3 Changes in shallow magma ascent between phases

The pumices erupted at the very start of phases C1, C2 and D are characterized by a combination of a significant increase in the subpopulation of large bubbles > 800 μm as well as a greater range of clast densities, with respect to the last erupted material from the preceding phases. These observations suggest that the magma first erupted in phases C1, C2 and D had a different and probably more complex shallow ascent history with respect to that discharged late in phases B, C1 and C2. The data are not compatible with the simple model that each of these phases began with arrival of a new pulse of magma with limited residence time in the shallow conduit and hence restricted opportunity for bubble

coalescence. Instead they suggest that the early erupted magma in C1, C2 and D1 was slightly more influenced by bubble interaction and coalescence than magma erupted late in these and the preceding phases; the reasons and implications are discussed below. Studies conducted by Carey et al., (in review) suggested three separate vent locations that were active in the eruption, centered upon the depressions indicated in Figure 3, which mimic NE-SW and SE-NW-trending structural faults. We suggest that the magma was intruded in cross-cutting elongated dike-like bodies centered on the NE-SW-trending Askja caldera marginal fault, and in a SE-NW-trending structural fault (Fig. 3). In our model, magma was able to reach shallow depths beneath any given portion of the vent system significantly before the onset of activity at that vent. The first magma erupted after the opening of a newly located vent (e.g. early C1 or D1 times) reflects this process, which led to extended residence times for the first-erupted magma compared to magma erupted during the peak discharge of each phase (Fig. 12a).

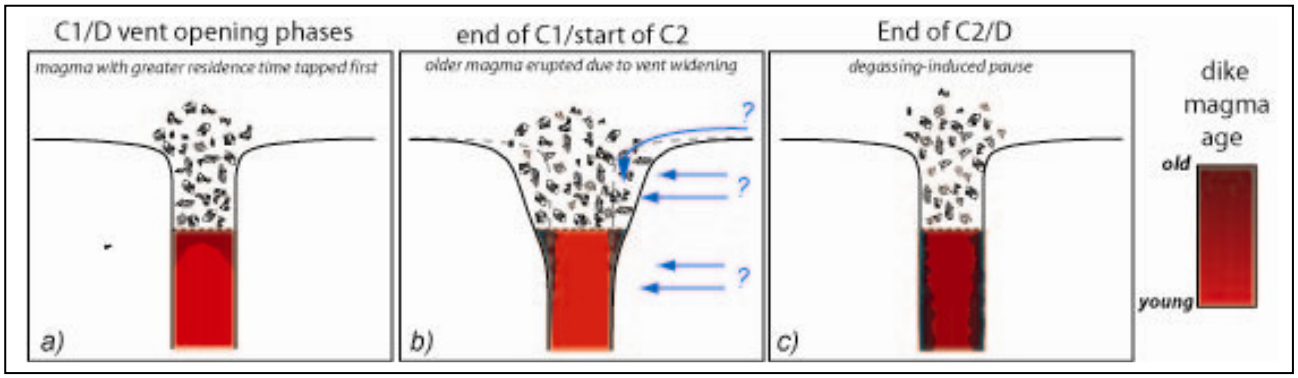

Figure 12: a) At the onset of the phreatoplinian and Plinian phases, magma with greater residence time in the conduit is erupted first (darker red), followed later by gas-rich magma (bright red). **(b)** During the phreatoplinian (C1) phase (1 hour), continued high ascent rates, water availability and vent widening facilitated a change from buoyant to collapsing column conditions. Throughout this period, magma with greater residence time at the margins of the conduit was removed. The timing and nature of the magma-water interaction is unknown and is currently being investigated. **(c)** At the end of the pyroclastic density current and Plinian phases, decreases of mass flux facilitated stagnation of magma on the conduit margins, prior to degassing-induced pauses in the eruption.

The vent active during C2 time is interpreted to be coincident with the C1 vent (Carey et al., in review). At the onset of C2, however, we see the greatest range of clast densities, a coarse population of bubbles similar to those observed at the onset of other phases and large, very complex bubbles with thick walls. The shift from buoyant plume to collapsing

column conditions appears not to be a result of a decrease in the mass flux as the bubble number densities (a proxy for decompression rate) are actually higher within the C2 phase (Table 3). Instead, we suggest that vent widening in the phreatoplinian phase changed exit conditions and led to the change in transport regime and the incorporation of magma with longer residence times from adjacent conduit and dike areas (Fig. 12b).

4.1.4 Changes in shallow magma ascent within a phase

Limited changes are observed in the clast density/bulk vesicularity and VVD data within phases. Throughout C1, we see an increase in the bubble number density through time, coupled with a decrease in the median size of the vesicles, and a decrease in the range of clast densities (Tables 2, 3). This trend is suggestive of higher rates of decompression, increasing rates of bubble nucleation during magma ascent (Mangan and Sisson, 2000). However, shallow processes of ascent must have been different; there is an obvious textural switch to a population of irregular distorted bubble shapes with thick bubble walls, despite an increase in the abundance of the small bubble populations (Fig. 5). These complex shapes suggest greater late-stage residence time of the majority of the magma despite higher early decompression rates and thus a decoupling of deep and shallow ascent processes. We suggest that this final phreatoplinian sample represents the beginning of vent widening (Fig. 12b). Magma that was residing in the adjacent dike had slightly longer residence times, and vent widening at the end of C1 led to the eruption of this magma and a shift from sustained buoyant to collapsing column conditions.

In the C2 phase, there is a trend with time of fluctuating median diameter and a non-uniform trend of vesicle volume distribution with a decrease in bubble number densities. In addition, there is an increase in the abundance of tube pumices (47 - 66 wt%) that are moderately to highly vesicular (83 % modal vesicularity). We suggest that slowed or stalled ascent in the shallow conduit during C2 facilitated variable degrees of bubble coalescence and collapse, and potentially, at times, a reduction in the effective radius of the conduit, inducing shearing of the bubbles. The final sample collected from this phase has an additional third linear segment representing coarse bubbles (Fig. 7; Table 4) and we suggest that this sample represents extended residence times in the conduit available for run-away coalescence and minor bubble collapse.

In the Plinian phase, there is a complex trend, slight fluctuations of bubble number density (with the exception of D5) and smaller median bubble sizes and ranges of clast densities in the D3 samples of this phase (Table 3). The highest number density and lowest median bubble size occurs in the UD3, suggesting that although early and late magma ascent conditions were fairly similar throughout this phase, the highest intensity of this phase correlates to this sample.

4.3 Pauses associated with the eruption

From eyewitness accounts there appear to have been two pauses during this eruption; the first between the subplinian (B) and phreatoplinian (C1) phases, and the second, at the end of the eruption (Carey et al., in review). Our limited microtextural data are based on a single subplinian sample which cannot demonstrate any change in the erupting magma that may have triggered this pause. Higher resolution sampling and textural analysis throughout the subplinian (B) deposits is required. Our analyses do suggest that there was the pause between pyroclastic density current (C2) and Plinian (D) phases was preceded by decreases in vesicle number density (i.e. decrease of decompression and magma ascent rates), and the pumice textures record progressively higher degrees of coalescence and shearing (Table 3). These observations support a degassing-driven pause between these two phases (Fig. 12c). The end of the eruption, characterized by the final Plinian (D5) pumice also has a much lower vesicle number density with high degrees of coalescence and shearing (Table 2), suggesting a degassing-induced end to the eruption (Fig. 12c).

4.4 Role of external water in highly explosive sustained wet volcanism

In addition to varying roles for early and late processes of nucleation, growth, coalescence and collapse that affect the vesicularity characteristics, could external factors such as the interaction of water induce texture contrasts between pumices erupted in wet and dry phases? The extent of vesiculation of the phreatomagmatic magma prior to fragmentation can be constrained by quantitative vesiculation data.

The density histograms of the Askja phreatomagmatic phases (C) are highly unimodal (Fig. 4a). Mean, modal and ranges of these clast vesicularities are also very similar to those of the earlier dry subplinian (B), and later Plinian (D) phases, suggesting that melt involved in the C phases had vesiculated to the same extent as that ejected in the 'dry'

eruptive phases (Table 3). The vesicle number densities in both the 1875 phreatomagmatic and Plinian phases are also very similar and, finally, the vesicle volume distributions all have similar broad ranges, from small 4 μm up to 5 mm bubbles (Fig. 8). These observations suggest that the processes of nucleation at depth, decompression and ascent rates were similar between wet and dry phases of the 1875 eruption. Based on the vesiculation data, textures and observations above, we suggest that the magma erupted during this phase was definitely at the peak of vesiculation at fragmentation. A characterization of the phreatoplinian ash morphology and pre- and post eruption volatile content of the phreatoplinian magma is now underway to further understand the timing of fragmentation and interaction of magma and water.

5.0 Conclusions

The 1875 eruption of Askja volcano is an excellent case study for examining conduit and vent dynamics, in particular shifts in eruption regime and transitions between wet and dry styles of activity. Carey et al., (in review), suggest multiple vent locations that were aligned in two cross-cutting weak structural zones trending NNE - SSW and NW - SE. We suggest that the magma erupted was intruded in a dike-like fashion along these two structural zones. External factors, including changing vent position, vent widening, and availability of external water, appear to be first-order influences facilitating rapid and reversible shifts in eruption styles. The initial shift from dry subplinian to wet phreatoplinian fall followed an increase in the eruption intensity coupled with a shift of vent location towards a source of high water availability. The vesicle number densities increase throughout the C1 phase; however, clast textures become increasingly complex, indicating a greater role and extended timescale for coalescence at shallow levels. We suggest that vent widening at the end of this phase facilitated incorporation of magma with longer residence times from adjacent portions of the dike system. The most complex and mature textures of all studied samples are from this period. The switch from wet sustained fall to wet density currents (C1 to C2) is superimposed on a continuous trend of inferred increasing decompression and magma ascent rates, suggesting that vent widening rather than a reduction of mass flux was responsible for this change in plume dynamics. The clast textures and density data also support this interpretation. Throughout

the density current phase, the vesicle number densities decrease; however, the deposit characteristics of the currents suggest lower degrees of water interaction with time. These combined observations suggest that at the end of the pyroclastic density current phase, the availability of water had greatly reduced at a time when magma flux was also declining. Pumice clast textures at the end of this phase suggest high degrees of coalescence and minor collapse, and support a degassing-induced pause in the eruption. The shift in eruption style from wet pyroclastic density currents to dry Plinian fall was due to both a shift in vent position away from the water source, and an increase in magma ascent rates. The end of this eruption is recorded in the pumice clast textures by an increase in the degree of coalescence and minor bubble collapse, we suggest that with time the magma in the shallow conduit was becoming increasingly outgassed and that this process ultimately led to the close of the Plinian phase of the eruption..

One important observation brought about by microscopic studies of pumice clasts of this eruption, is that degassing processes during deep and shallow magma ascent were decoupled within and between phases. At depth, nucleation and initial growth stages of growth were similar thorughtout the 1875 eruption; however, with continued ascent, shallow controls on degassing, changing vent position and vent widening severely affected the pumice clast textures and densities to differing degrees leading to textural diversity amongst the pyroclasts. The deposit characteristics together with textural observations of phreatomagmatic pumice clasts suggest that this magma was a foam prior to the interaction of water. Future studies are planned to examine the role of magma-water interaction for fragmentation during the sustained phreatoplinian phase.

Acknowledgements

This study was supported by NSF grants EAR-0310033 and EAR-0537459. Ármann Höskuldson participated in field work and contributed greatly to our understanding of the 1875 eruption. Many thanks to field supporters Tim Bowden (2004), Ben Sellers (2005), and Helena Buurman (2006) for their help. In addition we wish to thank Sarah Fagents and Lucia Gurioli for their insightful reviews of this manuscript. We thank and acknowledge the generosity of our hosts, the Nordic Volcanological Center, Institute of Earth Sciences, University of Iceland, with scientific and logistical support, and in

particular access to the Askja huts. We particularly thank Halldór Ólafsson and Eric Sturkell for their discussions and company in the field.

REFERENCES CITED

Adams, N.A., Houghton, B.F., Hildreth, W. 2006. Abrupt transitions during sustained explosive eruptions: examples from the 1912 eruption of Novarupta, Alaska. Bull Volc

Blower, J. D., Keating, J. P., Mader, H. M., and Phillips, J. C. 2002, The evolution of bubble size distributions in volcanic eruptions: J. Volcanol. Geotherm. Res. 120: 1-23.

Blower, J.D., Keating, J.P., Mader, H.M. and Phillips, J.C. 2001. Inferring volcanic degassing processes from vesicle size distributions. Geophys. Res. Lett. 28: 347-350.

Brandsdottir, B. 1992. Historical accounts of earthquakes associated with eruptive activity in the Askja volcanic system. Jökull, 42: 1-12.

Buttner, R., Dellino, P. and Zimanowski, B. 1999. Identifying magma-water interaction from surface features of ash particles. Nature, 401: 688-690.

Carey R.J., Houghton, B.F., Thordarson, T. 2008a. Complex welding of proximal Plinian deposits I: Regional welding. (in press). J.Volcanol. Geotherm. Res.

Carey R.J., Houghton, B.F., Thordarson, T. 2008b. Complex welding of proximal Plinian deposits II: Local welding (in press). J. Volcanol. Geotherm. Res.

Cashman KV, Mangan M 1994. Physical aspects of magmatic degassing. II. Constraints on vesiculation process from textural studies of eruptive products. *Rev. Mineral. 30*: 447-478.

Carey, R.J., Houghton, B.F., Thordarson, T. (in review). Tephra dispersal and eruption dynamics of the 1875 eruption of Askja volcano. Submitted to Bulletin of Volcanology, March 2008.

Cashman, K.V., Mangan, M.T.,1994. Physical aspects of magmatic degassing. II. Constrants on vesiculation processes from textural studies of eruptive products. In: Carroll MR, Holloway JR (eds) Volatiles in magmas. Rev. mineral 30:447-478.

Cole, P.D.Q., Wallenstein, N. Gaspar, J.L, Duncan, A.M. Guest, J.E. 1995. An historic subplinian/phreatomagmatic eruption; the 1630AD eruption of Furnas volcano, Sao Miguel, Azores. J. Volcanol. Geotherm. Res. 69: 117-135.

Gardner, J.E., Hilton, M. and Carroll, M.R. 1999. Experimental constraints on degassing of magma: isothermal bubble growth during continuous decompression from high pressure. Earth and Planetary Science Letters, 168: 201-218.

Gaonac'h, H., Lovejoy, S., Stix, J., Scherzter, D. 1996. A scaling growth model for bubbles in basaltic lava flows. Earth and Planetary Science Letters 139: 395-409.

Gurioli, L., Houghton, B.F., Cashman, K.V., Cioni, R. 2005. Complex changes in eruption dynamics during the 79 AD eruption of Vesuvius. Bull. Volcanol. 67: 144-159.

Heiken, G. 1987. Textural analysis of tephra from a rhyodacitic eruption sequence, Thira (Santorini), Greece. In Marshall J (Ed.), Clastic Particles, Van Nostrand-Reinhold Co., New York, pp. 67-78.

Heiken, G., Wohletz, K. 1985. Volcanic Ash. University of California Press, Berkley, 246 pp.

Heiken, G. 1972. Morphology and Petrography of Volcanic ashes. Geol. Soc. Amer. Bull. 83:1962-1986.

Houghton B.F, Wilson C.J.N. 1989. A vesicularity index for pyroclastic deposits. Bull. Volcanol. 51: 451-462.

Houghton, B.F., et al., 1995. Chronology and dynamics of a large silicic magmatic system: central Taupo Volcanic Zone, New Zealand. Geology, Boulder, 23: 13-16.

Houghton, B. F., Hobden, B.J., Cashman, K.V., Wilson, C.J.N, Smith, R.T. 2003. Large-scale interaction of Lake water and Rhyolitic magma during the 1.8 ka Taupo eruption, New Zealand.

Hurwitz, S., Navon, O. 1994. Bubble nucleation in rhyolitic melts: Experiments at high pressure, temperature, and water content. Earth and Planetary Science Letters 122: 267-280.

Johnstrup, F., 1877. Om de året 1875 forefaldne vulcanske udbrud paa Island. Geografisk Tidsskrift, 1: 50-66.

Klug C, Cashman K.V. 1994. Vesiculation of May 18, 1980 Mount St. Helens magma. Geology 22:468-472.

Klug, C., Cashman, K. V., and Bacon, C. R., 2002, Structure and physical characteristics of pumice from the climactic eruption of Mount Mazama (Crater Lake), Oregon. Bull. Volcanol. 64: 486-501.

Larsen, G., Thorarinsson, S. 1977. H4 and other acid Hekla tephra layers. Jokull, 27: 28-46.

Lyakhovsky, V., Hurwitz, S., Navon, O., 1996. Bubble growth in rhyolitic melts: experimental and numerical investigation. Bull.Volcanol. 58: 19-32.

Mangan, M.T., Cashman, K.V. 1996. The structure of basaltic scoria and reticulatie and inferences for vesiculation, foam formation and fragmentation in lava fountains. J. Volcanol. Geotherm. Res. 73: 1-18.

Mangan, M.T., Mastin, L., Sisson, T., 2004a. Gas evolution in eruptive conduits: combining insights from high temperature and pressure decompression experiments with steady-state flow modeling. J. Volcanol. Geotherm. Res. 129: 23-36.

Mangan, M.T., Sisson, T. and Hankins, W.B., 2004b. Decompression experiments identify kinetic controls on explosive silicic eruptions. Geophys. Res. Lett. 31(L08605): 1-5.

Mangan, M.T. and Sisson, T.W. 2000. Delayed, disequilibrium degassing in rhyolite magma: decompression experiments and implications for explosive volcanism. Earth and Planetary Science Letters. 183: 441-455.

Mitchell, K. 2005. Coupled conduit flow and shape in explosive volcanic eruptions. J. Volcanol. Geotherm. Res. 143, 187-203.

Navon, O., Lyakhovsky, V. 1998. Vesiculation processes in silicic magmas. In: Physics of Explosive Volcanism, eds. JS Gilbert and RSJ Sparks, Geol. Soc. Lond. Spec. Publ. 145:27-50.

Mourtada-Bonnefoi, C.C., Laporte, D. 1999. Experimental study of homogeneous bubble nucleation in rhyolitic magmas. Geophys Res. Lett 26: 3505-3508.

Orsi, G., Gallo, G., Heiken, G., Wohletz, K., Yu, E., Bonani, G. 1992. A comprehensive study of pumice formation and dispersal: the Cretaio tephra of Ischia (Italy). J. Volcanol. Geotherm. Res. 53:329-354.

Polacci, M., Pioli, L., Rosi, M. 2003. The Plinian phase of the Campanian Ignimbrite eruption (Phlegrean Fields, Italy): evidence from density measurements and textural characterization of pumice. Bull. Volcanol. 65: 418-432.

Polacci, M., Papale, P. and Rosi, M. 2001. Textural heterogeneities in pumices from the climactic eruption of Mount Pinatubo, 15 June 1991, and implications for magma ascent dynamics. Bull. Volcanol. 63: 83-97.

Rosi, M., Paladio-Melosantos, M.L., Dimuro, A., Leoni, R. and Bacolcol, T. 2001. Fall vs flow activity during the 1991 climactic eruption of Pinatubo Volcano (Philippines). Bull. Volcanol. 62: 549-566.

Sable, J.E., Houghton, B.F., Del Carlo, P., Coltelli, M., 2006. Cross-conduit heterogeneity and shifting degassing behavior during the Etna 122 BC basaltic plinian eruption. J. Volcanol. Geotherm. Res. (in review).

Sahagian, D.L., Proussevitch, A.A., 1998. 3D particle size distributions from 2D observations: stereology for natural applications. J. Volcanol. Geotherm. Res. 84: 173- 196.

Self, S. and Sparks, R.S.J. 1978. Characteristics of widespread pyroclastic deposits formed by the interaction of silicic magma and water. Bull. Volcanol. 41: 196-212.

Sigurdsson, H. and Sparks, R.S.J. 1978a. Rifting episode in north Iceland in 1874-1875 and the eruptions of Askja and Sveinagjá. Bull. Volcanol. 41: 1-19.

Sigurdsson, H. and Sparks, R.S.J. 1981. Petrology of rhyolitic and mixed magma ejecta from the 1875 eruption of Askja, Iceland. J. Petrol. 22: 41-84.

Sigvaldason, G.E., 1979. Rifting, magmatic activity, and interaction between acid and basic liquids: The 1875 Askja eruption in Iceland. 7903, Nordic Volcanological Institute, Reykjavik, Iceland

Sigvaldason, G.E. 2002. Volcanic and tectonic processes coinciding with glaciation and crustal rebound: an early Holocene rhyolitic eruption in the Dyngjufjoll volcanic centre and the formation of the Askja caldera, north Iceland. Bull.Volcanol. 64: 192-205.

Sigurdsson H., Carey, S., Cornell, W., Pescatore, T. 1985. The eruption of Vesuvius in A.D. 79. Nat. Geograph. Res. 1: 332-387.

Simakin, A.G., Armienti, P., Epelbaum, M.B. 1999. Coupled degassing and crystallization: experimental study at continuous pressure drop, with application to volcanic bombs. Bull. Volcanol. 61: 275-287.

Sparks, R.S.J., Wilson, L., Sigurdsson, H. 1981. The pyroclastic deposits of the 1875 eruption of Askja, Iceland. Phil. Trans. Roy. Soc. Lond. Series A, 299: 241-273.

Thordarson, T., Carey, R.J., Houghton, B.F. (in prep). Historical accounts of 19th and 20th century volcanic eruptions at the Askja volcano (Iceland) with a special reference to the 1874-1876 volcano-tectonic event.

Whitham, A.G., Sparks, R.S.J. 1986. Pumice. Bull. Volcanol. 48: 209-223.

Wilson, L., Sparks, R.S.J., Walker, G.P.L. 1980. Explosive volcanic eruptions - IV. The control of magma properties and conduit geometry on eruption column behaviour. Geophys. J. Royal Astronom. Soc. 63: 117-148.